

Spin and density excitations of one-dimensional self-bound Bose-Bose droplets

Ritu,^{1,*} Rajat,^{1,2,†} Manpreet Singh,^{1,‡} Rajesh Kumar Gupta,^{1,§} and Sandeep Gautam^{1,¶}

¹*Department of Physics, Indian Institute of Technology Ropar, Rupnagar 140001, Punjab, India*

²*Department of Physics, Ben-Gurion University of the Negev, Beer-Sheva 84105, Israel*

We study density and spin excitations of one-dimensional self-bound Bose-Bose droplets within Bogoliubov theory, and show that spin excitations come alive, especially as the interspecies coupling is made less attractive. We argue that spin excitations are particularly relevant in the one-dimensional droplet regime, where droplets are realized within the mean-field stability regime, as has been confirmed by the Quantum Monte Carlo simulations. As the interspecies coupling strength increases within the mean-field stability regime, spin modes ultimately fall below the particle-emission threshold, thus becoming observable in the droplet spectrum. We analyze the Bogoliubov model for both pseudospinor and population-imbalanced scalar mixtures, encompassing both the density and spin sectors, and corroborate our findings through variational analysis of density and spin breathing modes, as well as real-time dynamics. Additionally, we compare our results with Petrov's "original" theory, which considers the Lee-Huang-Yang (LHY) correction at the attractive edge of the mean-field stability regime and a beyond-LHY description of Bose-Bose mixtures.

I. INTRODUCTION

Quantum droplets are a self-bound phase of ultracold quantum gases that arises from beyond-mean-field effects. This phase was first predicted by Petrov [1] and was later experimentally realized in homonuclear mixtures of two components [2–5] and heteronuclear mixtures [6–8], as well as in dipolar Bose-Einstein condensates (BECs) [9–12]. Droplets are stabilized when the mean-field interactions and Lee-Huang-Yang (LHY) correction provide competing contributions to the energy density, preventing the mean-field collapse in these systems [1, 13].

In three dimensions, the LHY term is repulsive, so droplets require net attractive mean-field interactions or $\delta g = g + g_{12} < 0$, $|\delta g| \ll g$, where g and g_{12} are the intra- and interspecies coupling constants, respectively [1]. The LHY energy can be written as a sum over zero-point energies of Bogoliubov modes; however, for $\delta g < 0$ the density (in-phase) branch is dynamically unstable with square of speed of sound $c_d^2 \sim n\delta g$, while the spin (out-of-phase) branch remains stable with $c_s^2 \sim n(g - g_{12}) > 0$, where n is the total density [14, 15]. Including both branches naively yields an unphysical complex LHY energy [1, 16]. Petrov's prescription avoids this by discarding the density-branch contribution (often phrased as setting the sound speed for density mode to zero) and retaining only the stable branch when constructing the LHY energy [1]. A generalization of Bogoliubov theory with the inclusion of bosonic pairing [17, 18], and beyond Bogoliubov theories [16, 19] have also been proposed to remedy the issue of imaginary c_d . These theories have been shown to agree better with diffusion Monte Carlo for equilibrium densities of the droplets, especially as δg becomes more negative [20]. The net effective mean-field attraction required for the realization of a three-dimensional (3D) droplet ensures that

spin excitations, lying above the particle emission threshold, are absent from the excitation spectrum of spherical droplets [21–24].

Quantum fluctuations also lead to the droplet phase in two-dimensional (2D) Bose-Bose mixtures with weak interspecies attraction and weak intraspecies repulsion [13, 25]. The 2D quantum droplets hosting vortices [26], vortex clusters under rotating confinements [27, 28], and a variety of other nonlinear excitations [29] have been theoretically studied in addition to studies of modulation instability [30] and excitation spectrum [31–33].

In contrast to 3D and 2D, one-dimensional (1D) droplets are stabilized by the attractive LHY correction balancing the net mean-field repulsion ($\delta g > 0$) [25]. The droplets are therefore realized within the mean-field stability regimes with a stable density phonon mode, removing any need to ignore its contribution to the LHY correction [16]. Most of the studies on 1D droplets still consider an approximate LHY correction evaluated at $g_{12} = -g$ as per Petrov's original theory, which makes the corresponding description suitable for $0 < \delta g \ll g$. At $\delta g \gtrsim 0$, the spin excitations lie above the particle emission threshold, allowing a single-component description of 1D droplets [25, 34, 35]. The single-component description of 1D droplets has been used to study ground states [25], excitation spectrum [34–36], collision dynamics [35], and solitary waves [37, 38]. As δg increases within the mean field stability regime, spin excitations soften and may lie below the particle emission threshold. In this regime, one has to treat the droplet as a genuine two-component system with accessible density and spin excitations. The two-component description, albeit with an approximate LHY correction (Petrov's theory), has been used to study the rotational properties of scalar Bose-Bose mixtures confined on a ring with a particle imbalance [39]. The description has also been used to study the stability of 1D droplets under weak harmonic confinement in scalar mixtures with a particle imbalance [40]. The LHY corrections for a weakly interacting single-component Bose gas and Bose-Bose mixtures across the crossover from 3D to 2D and 3D to 1D have also been calculated [41–43].

The impact of beyond LHY correlations on the ground state and the dynamics of 1D droplets have been studied using an

* ritu.22phz0002@iitrpr.ac.in

† rajat13sep@gmail.com

‡ manpreet.25phz0008@iitrpr.ac.in

§ rajesh.gupta@iitrpr.ac.in

¶ sandeep@iitrpr.ac.in

ab initio nonperturbative approach [44–46]. Moreover, several theoretical frameworks have been used to study the liquid-to-gas transition in 1D Bose-Bose mixtures, including quantum Monte Carlo methods [47, 48], inclusion of beyond-LHY effects [16], and a generalization of Bogoliubov theory with the inclusion bosonic pairing field [18].

Recently, Ref. [49] discussed the comparison between the ground state density profiles obtained with Petrov’s and Bogoliubov theories across the entire mean-field stability regime. These theories match at $\delta g = 0$, and as δg is increased, the former significantly overestimates the finite-sized droplets’ saturation densities, confining them over a smaller extent. In this work, we use the Bogoliubov theory with exact LHY correction to calculate the density and spin excitations of 1D Bose-Bose droplets. The spin excitations have hardly been studied in Bose-Bose droplets, irrespective of the theory employed or the dimensionality of the system. We calculate the full excitation spectrum from the numerical solutions of Bogoliubov equations and analyze the lowest-lying density- and spin-breathing modes using a variational analysis. We consider both self-bound pseudospinor and population-imbalanced scalar Bose-Bose mixtures. The results of Bogoliubov theory are compared with those from Petrov’s theory and, in addition, for the density-breathing mode, with a beyond-LHY theory.

The paper is organized as follows. We introduce the Bogoliubov theory used for the description of 1D Bose-Bose mixtures and contrast it with Petrov’s original prescription in Sec. II. We discuss pseudospinor Bose-Bose mixtures, revisiting a simpler description, which ignores the spin excitations, and later their excitations are obtained numerically using a full two-component description and supported by a variational analysis in Sec. III. This is followed by a discussion on the excitations in a scalar Bose-Bose mixture in Sec. IV. We then discuss a beyond-LHY description of 1D Bose-Bose mixtures to examine the liquid-to-gas transition and the density breathing mode in Sec. V. We summarize this work in Sec. VI.

II. MODEL

We consider a 1D two-component weakly interacting Bose-Bose mixture within the framework described by the Bogoliubov approximation [13, 25]. The energy density of such a homogeneous mixture with equal masses of the two species is [25]

$$\mathcal{E} = \frac{1}{2} \sum_{\nu\nu'} g_{\nu\nu'} n_\nu n_{\nu'} - \frac{2\sqrt{m}}{3\hbar\pi} \sum_{\pm} c_{\pm}^3, \quad (1)$$

where ν and ν' are the labels (1 or 2) of the two components, $g_{\nu\nu'}$ denotes the coupling constants, n_ν is the density of the species ν , and c_{\pm} are the two sound velocities. We consider the system in the weak coupling limit, for which the dimensionless parameter $n|a_{\nu\nu'}| \gg 1$, where $n = \sum_{\nu} n_\nu$ and $a_{\nu\nu'}$ are s -wave scattering lengths related with coupling constants as $g_{\nu\nu'} = -2\hbar^2/ma_{\nu\nu'}$ [25, 47]. In Eq. (1), the first term is the mean-field contribution to the energy density, and the

second is the LHY correction arising from the quantum fluctuations with c_{\pm}^2 given as

$$c_{\pm}^2 = \frac{g_{11}n_1 + g_{22}n_2 \pm \sqrt{(g_{11}n_1 - g_{22}n_2)^2 + 4g_{12}^2n_1n_2}}{2}. \quad (2)$$

The finite-sized self-bound solutions (solitons or droplets) of the system can be described by the Lagrangian

$$L = \int dx \left[\sum_{\nu} \left\{ \frac{i\hbar}{2} \left(\Phi_{\nu}^* \frac{\partial \Phi_{\nu}}{\partial t} - \Phi_{\nu} \frac{\partial \Phi_{\nu}^*}{\partial t} \right) - \frac{\hbar^2}{2m} \left| \frac{d\Phi_{\nu}}{dx} \right|^2 \right\} - \mathcal{E} \right], \quad (3)$$

where $\Phi_{\nu}(x, t)$ are the component wavefunctions with $|\Phi_{\nu}(x, t)|^2 = n_{\nu}(x, t)$. The Euler-Lagrange or Gross-Pitaevskii (GP) equations describing the dynamics of the system are [49]

$$i\hbar \frac{\partial \Phi_{\nu}}{\partial t} = \left(-\frac{\hbar^2}{2m} \frac{\partial^2}{\partial x^2} + g_{\nu\nu} |\Phi_{\nu}|^2 + g_{\nu\bar{\nu}} |\Phi_{\bar{\nu}}|^2 + \Delta\mu_{\nu} \right) \Phi_{\nu}, \quad (4)$$

where $\bar{\nu} = 1, 2$ and $\bar{\nu} \neq \nu$ and

$$\begin{aligned} \Delta\mu_{\nu} &= -\frac{\sqrt{m}}{\pi\hbar} \sum_{\pm} c_{\pm}^2 \frac{\partial c_{\pm}^2}{\partial n_{\nu}}, \\ &= -\frac{\sqrt{m}(g_{11}n_1 + g_{22}n_2)}{4\pi\hbar} \\ &\quad \times \left[3g_{\nu\nu} \mathcal{R}(p) + 2(g_{11}n_1 + g_{22}n_2) \frac{\partial \mathcal{R}}{\partial p} \frac{\partial p}{\partial n_{\nu}} \right], \end{aligned} \quad (5)$$

is the LHY correction term. In Eq. (6), p and $\mathcal{R}(p)$ are defined as

$$p = \frac{4(g_{12}^2 - g_{11}g_{22})n_1n_2}{(g_{11}n_1 + g_{22}n_2)^2}, \quad (7a)$$

$$\mathcal{R}(p) = \frac{\sqrt{2}}{3} \left((1 - \sqrt{p+1})^{\frac{3}{2}} + (1 + \sqrt{p+1})^{\frac{3}{2}} \right). \quad (7b)$$

If $\mathcal{R}(p)$ in Eq. (7b) is evaluated at the attractive edge of the mean-field stability regime, i.e., $g_{12} = -\sqrt{g_{11}g_{22}}$ or $p = 0$, Eq. (4) reduces to one obtained by Petrov *et al.* in Ref. [25],

$$\begin{aligned} i\hbar \frac{\partial \Phi_{\nu}}{\partial t} &= \left(-\frac{\hbar^2}{2m} \frac{\partial^2}{\partial x^2} + g_{\nu\nu} |\Phi_{\nu}|^2 + g_{\nu\bar{\nu}} |\Phi_{\bar{\nu}}|^2 \right. \\ &\quad \left. - \frac{\sqrt{m}g_{\nu\nu}}{\hbar\pi} \sqrt{g_{11}|\Phi_1|^2 + g_{22}|\Phi_2|^2} \right) \Phi_{\nu}. \end{aligned} \quad (8)$$

We refer to Eqs. (4) and (8) as Bogoliubov’s and Petrov’s models/theories, respectively. It is to be noted that the LHY correction within Bogoliubov theory depends on g_{12} , unlike Petrov’s theory. In this work, we consider pseudospinor and scalar Bose-Bose mixtures. If N_{ν} denotes the number of particles of species ν and $N = \sum_{\nu} N_{\nu}$ is the total number particles

in a finite-sized droplet, then

$$\int \sum_{\nu} |\Phi_{\nu}(x, t)|^2 dx = N, \quad (9)$$

for a pseudospinor mixture, whereas

$$\int |\Phi_{\nu}(x, t)|^2 dx = N_{\nu}, \quad (10)$$

for a scalar mixture. To calculate the excitation spectrum, we linearize Eqs. (4) by considering fluctuation around the

ground state $\phi_{\nu}(x)$ using

$$\Phi_{\nu}(x, t) = e^{-\mu_{\nu}t} [\phi_{\nu}(x) + \delta\phi_{\nu}(x, t)], \quad (11)$$

where μ_{ν} are the chemical potentials; $\mu_1 = \mu_2 = \mu$ for a pseudospinor mixture. Then, using the Bogoliubov transformation,

$$\delta\phi_{\nu}(x, t) = \sum_l [u_{\nu}^l(x) e^{-i\omega_l t} - v_{\nu}^{l*}(x) e^{i\omega_l t}], \quad (12)$$

we obtain the Bogoliubov-de-Gennes (BdG) as

$$\begin{pmatrix} \mathcal{M} & -g_{11}\phi_1^2 - B_{11} & g_{12}\phi_1\phi_2^* + A_{21} & -g_{12}\phi_1\phi_2 - B_{21} \\ g_{11}\phi_1^2 + B_{11}^* & -\mathcal{M}^* & g_{12}\phi_1\phi_2^* + A_{21} & -g_{12}\phi_1\phi_2 - B_{21} \\ g_{21}\phi_2\phi_1^* + A_{12} & -g_{21}\phi_2\phi_1 - B_{12} & \mathcal{N} & -g_{22}\phi_2^2 - B_{22} \\ g_{21}\phi_2^*\phi_1^* + B_{12}^* & -g_{21}\phi_2^*\phi_1 - A_{12}^* & g_{22}\phi_2^{*2} + B_{22}^* & -\mathcal{N}^* \end{pmatrix} \begin{pmatrix} u_1^l \\ v_1^l \\ u_2^l \\ v_2^l \end{pmatrix} = \omega_l \begin{pmatrix} u_1^l \\ v_1^l \\ u_2^l \\ v_2^l \end{pmatrix}, \quad (13)$$

where elements \mathcal{M} , \mathcal{N} , A , and B for the two models are defined by Eqs. (42), (43) and (44) in the Appendix. The quasi-particle wave functions satisfy the normalization condition

$$\sum_{\nu} \int dx [|u_{\nu}^l(x)|^2 - |v_{\nu}^l(x)|^2] = 1, \quad (14)$$

where l represents the eigenvalue index corresponding to energy ω_l with u_{ν}^l and v_{ν}^l as quasi-particle wave functions.

III. TWO-COMPONENT PSEUDOSPINOR MIXTURE

Bogoliubov theory within single-mode approximation:— In a 1D pseudospinor mixture near the attractive edge of the mean field stability regime, where $0 < \delta g = g_{12} + \sqrt{g_{11}g_{22}} \ll \sqrt{g_{11}g_{22}}$, the spin excitations are energetically costlier relative to the density excitations and may well lie above the particle emission threshold $\sim |\delta g|n$ for δg close to zero. In this regime, the ground state structure and low-lying density excitations can be studied within a simpler framework provided by the single-mode approximation (SMA) [1, 25, 34, 35]. The SMA entails that the component wavefunctions are proportional to a single wave function, i.e., $\Phi_{\nu}(x, t) = \alpha_{\nu}\Phi(x, t)$, where $|\Phi|^2 = \sum_{\nu} n_{\nu} = n$ and α_{ν} are c numbers with $\sum_{\nu} |\alpha_{\nu}|^2 = 1$. The constant density ratio $n_1/n_2 = |\alpha_1|^2/(1-|\alpha_1|^2) = \beta$ within SMA. To calculate β , we rewrite the energy density of the homogeneous mixture within the Bo-

goliubov theory

$$\begin{aligned} \mathcal{E} &= \frac{(g_{11}n_1^2 + g_{22}n_2^2)}{2} + g_{12}n_1n_2 - \frac{\sqrt{m}(g_{11}n_1 + g_{22}n_2)^{\frac{3}{2}}}{2\hbar\pi} \\ &\times \mathcal{R}(p), \quad (15a) \\ &= \frac{n^2(g_{11}\beta^2 + g_{22} + 2g_{12}\beta)}{2(\beta + 1)^2} - \frac{\sqrt{m}(g_{11}\beta + g_{22})^{\frac{3}{2}}n^{\frac{3}{2}}}{2\hbar\pi\sqrt{(\beta + 1)^3}} \\ &\times \mathcal{R}(\zeta), \quad (15b) \end{aligned}$$

where $\zeta = 4\beta(g_{12}^2 - g_{11}g_{22})/(g_{11}\beta + g_{22})^2$, whereas the meanfield energy density within Petrov's theory corresponds to $\zeta = 0$ or $\mathcal{R}(\zeta = 0) = 4/3$ in Eq. (15b). The minimization of energy per particle, $\mathcal{E}(n, \beta)/n$, with respect to (n, β) for fixed g_{11}, g_{22} , and g_{12} yields the saturation density of the flat-top droplets and the precise density ratio. In Refs. [1, 25, 34, 35], the density locking condition has been approximated as $n_1/n_2 = \sqrt{g_{22}/g_{11}}$, which holds true at $\delta g = 0$ or trivially for $g_{11} = g_{22}$, to arrive at an effective single component description. We show the density ratio based on the numerical minimization of $\mathcal{E}(n, \beta)/n$, for Bogoliubov and Petrov's theories, in Fig. 1 for $g_{12} = -0.6g_{22}$ as a function of g_{11}/g_{22} . The β values are in very good agreement with the density ratio measured at the center of the finite-sized self-trapped solutions obtained by numerically solving the GP Eqs. (4) and (8), for Bogoliubov and Petrov's theories, respectively, and start deviating from the simpler estimate $\sqrt{g_{22}/g_{11}}$ with an increase in asymmetry between intraspecies couplings.

For finite-sized self-bound solutions within SMA, Lagrangian in Eq. (3) with $\Phi_{\nu}(x, t) = \alpha_{\nu}\Phi(x, t)$ and energy density in Eq. (15b) leads to a single Euler-Lagrange or GP

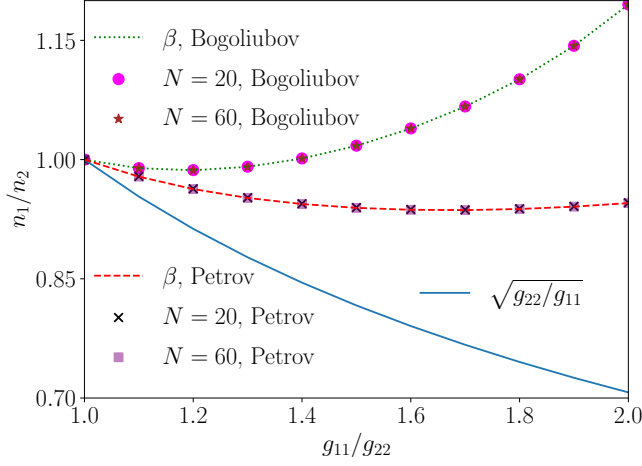


FIG. 1. Density ratio $\beta = n_1/n_2$ obtained by a minimization of the energy per particle $\mathcal{E}(n, \beta)/n$ as a function g_{11}/g_{22} for $g_{12} = -0.6g_{22}$ for Bogoliubov and Petrov's theories. Symbols denote the density ratio at the center of the finite-sized self-trapped solutions with $N = 20$ and 60 obtained by numerically solving the GP Eqs. (4) for Bogoliubov and (8) for Petrov's theory. For comparison, the simpler estimate of density ratio $\sqrt{g_{22}/g_{11}}$, which minimizes the mean-field energy density for $g_{12} = -\sqrt{g_{11}g_{22}}$ is also shown.

equation

$$i\hbar \frac{\partial \Phi(x, t)}{\partial t} = \left(-\frac{\hbar^2}{2m} \frac{\partial^2}{\partial x^2} + \frac{g_{11}\beta^2 + g_{22} + 2g_{12}\beta}{(\beta + 1)^2} |\Phi(x, t)|^2 - \frac{3\sqrt{m(g_{11}\beta + g_{22})^3}}{4\hbar\pi\sqrt{(\beta + 1)^3}} |\Phi|\mathcal{R}(\zeta) \right) \Phi(x, t). \quad (16)$$

To cast the above equation in dimensionless form, we first rescale the wavefunction as $\Phi = \Phi_0 \tilde{\Phi}$ with

$$\Phi_0 = \frac{3\sqrt{m(\beta + 1)(g_{11}\beta + g_{22})^3}\mathcal{R}(\zeta)}{4\pi\hbar(g_{11}\beta^2 + g_{22} + 2g_{12}\beta)}, \quad (17)$$

and then consider

$$l_0 = \frac{4\hbar^2\pi\sqrt{(\beta + 1)(g_{11}\beta^2 + g_{22} + 2g_{12}\beta)}}{3m\sqrt{(g_{11}\beta + g_{22})^3}\mathcal{R}(\zeta)}, \quad (18a)$$

$$t_0 = \frac{16\hbar^3\pi^2(\beta + 1)(g_{11}\beta^2 + g_{22} + 2g_{12}\beta)}{9m(g_{11}\beta + g_{22})^3[\mathcal{R}(\zeta)]^2}, \quad (18b)$$

$$E_0 = \frac{\hbar^2}{ml_0^2} = \frac{\hbar}{t_0} = \frac{9m(g_{11}\beta + g_{22})^3[\mathcal{R}(\zeta)]^2}{16\hbar^2\pi^2(\beta + 1)(g_{11}\beta^2 + g_{22} + 2g_{12}\beta)}, \quad (18c)$$

as units of length, time, and energy, respectively. The dimensionless equation thus obtained is

$$i \frac{\partial \tilde{\Phi}}{\partial \tilde{t}} = \left(-\frac{1}{2} \frac{\partial^2}{\partial \tilde{x}^2} + |\tilde{\Phi}|^2 - |\tilde{\Phi}| \right) \tilde{\Phi}, \quad (19)$$

where $\tilde{x} = x/l_0$, $\tilde{t} = t/t_0$, and the number of particles $\tilde{N} = \int |\tilde{\Phi}|^2 d\tilde{x}$ is in units of

$$N_0 = \Phi_0^2 l_0 = \frac{3\sqrt{(g_{11}\beta + g_{22})^3(\beta + 1)^3}\mathcal{R}(\zeta)}{4\pi\sqrt{(g_{11}\beta^2 + g_{22} + 2g_{12}\beta)^3}}. \quad (20)$$

For equal intraspecies couplings, $g_{11} = g_{22} = g$, $\beta = 1$ and $\zeta = g_{12}^2/g^2 - 1$, which fixes l_0 , t_0 , E_0 , and Φ_0 in terms of coupling strengths. The exact self-bound solution of Eq. (19) is [25, 35]

$$\tilde{\Phi}(\tilde{x}, \tilde{t}) = -\frac{3\tilde{\mu}e^{-i\tilde{\mu}\tilde{t}}}{1 + \sqrt{1 + \frac{9\tilde{\mu}}{2}} \cosh(\sqrt{-2\tilde{\mu}}\tilde{x}^2)}, \quad (21)$$

with the number of atoms

$$\tilde{N} = \frac{4}{3} \left(\ln \frac{\sqrt{-9\tilde{\mu}/2} + 1}{\sqrt{9\tilde{\mu}/2} + 1} - \sqrt{-\frac{9\tilde{\mu}}{2}} \right). \quad (22)$$

The form of Eq. (19) matches the single GP equation derived by Petrov *et al.* [25, 34, 35], for which meanfield energy \mathcal{E} can be obtained from Eq. (15b) and respective units of various quantities from Eqs. (17), (18), and (20) by substituting $\beta = \sqrt{g_{22}/g_{11}}$ and evaluating $\mathcal{R}(\zeta)$ at $\zeta = 0$. The BdG equations corresponding to the linearization of the single GP equation (19) for this case have been used to calculate density excitations in a pseudospinor mixture with equal intraspecies couplings [34–36].

Excitation spectrum of pseudospinor Bose-Bose droplet

To describe the complete dynamics or excitation spectrum of a pseudospinor mixture as δg increases from zero, SMA needs to be abandoned in favor of the dynamics described by the full model, viz. Eqs. (4) and (13). In this direction, we cast these equations in dimensionless form by expressing length, time, energy, and Φ_ν in units of \hbar^2/mg , \hbar^3/mg^2 , mg^2/\hbar^2 , and \sqrt{mg}/\hbar , respectively, where $g = \sqrt{g_{11}g_{22}}$.

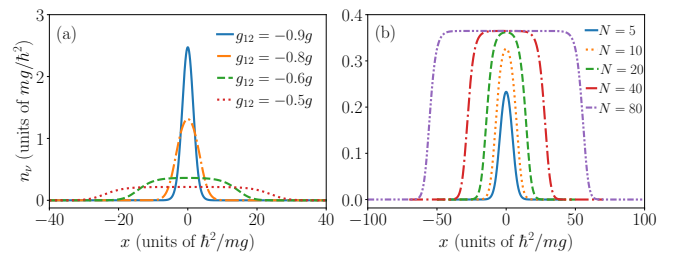


FIG. 2. The density profiles of the self-bound ground-state solutions of the Bogoliubov model, viz. Eqs. (4), for equal intraspecies coupling strengths, $g_{11} = g_{22} = g$. Component density for (a) $N = 20$ and (b) $g_{12} = -0.6g$, where $n_1(x) = n_2(x)$.

Numerical results:— We consider $g_{11} = g_{22} = g > 0$ for the pseudospinor mixture and solve Eqs. (4) numerically using split-time step imaginary time propagation [50] to obtain

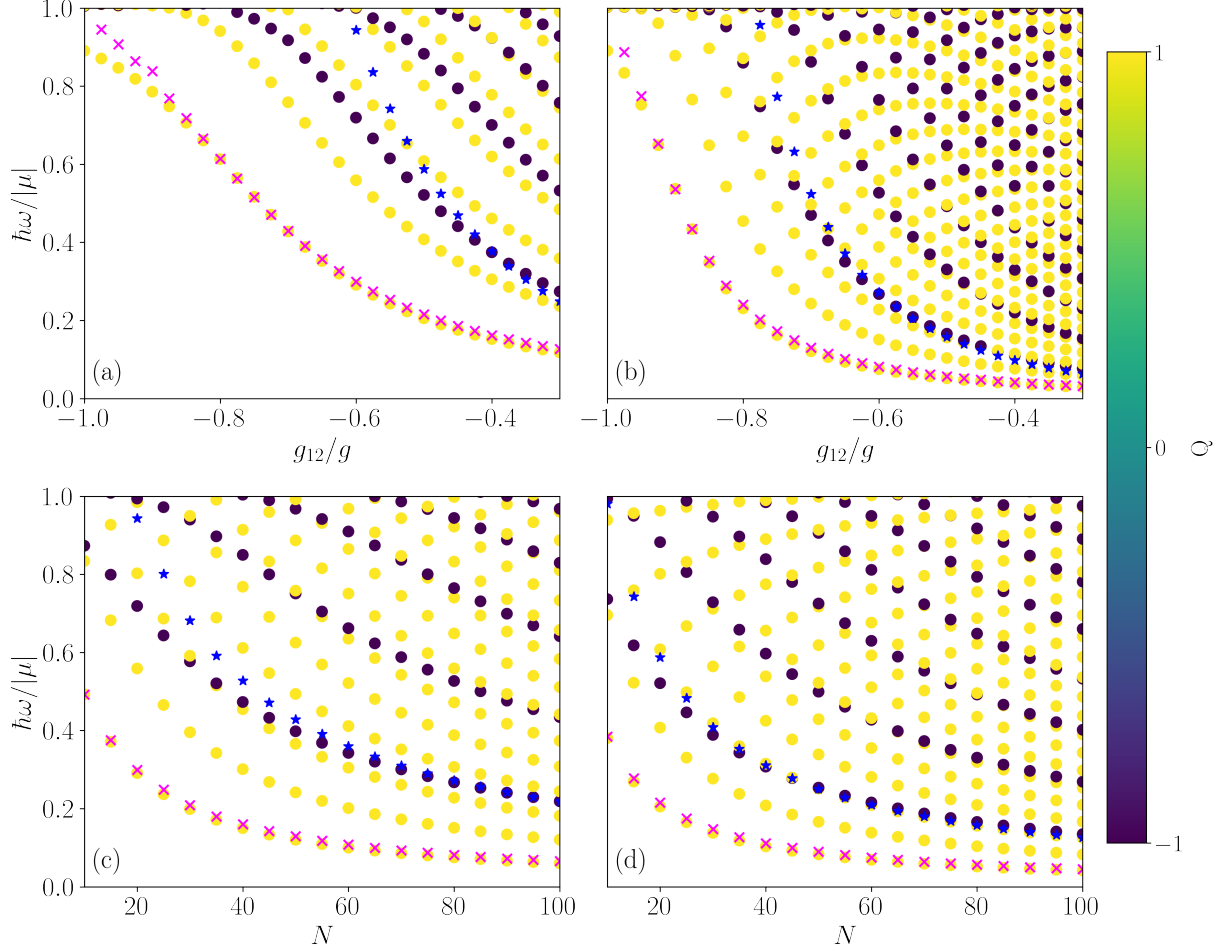


FIG. 3. (a)-(d) Solid circles are excitation energies calculated by solving BdG Eqs. (13) for the Bogoliubov model. (a) and (b): Excitation energies as a function of g_{12}/g for (a) $N = 20$ and (b) $N = 80$. (c) and (d): Excitation energies as a function of N for (c) $g_{12} = -0.6g$ and (d) $g_{12} = -0.5g$. Dark (dark-blue) and light (yellow) solid circles correspond to spin and density modes, respectively. ‘Cross’ and ‘star’ symbols are the energies of density- and spin-breathing modes, respectively, obtained from the variational analysis. The energies are in units of particle emission threshold $|\mu|$, and only the energies below the emission threshold are shown.

the ground state solutions. Changes in the density profile of the ground state of the mixture with an increase in g_{12} for fixed N or with an increase in N for fixed g_{12} are shown in Figs. 2(a) and 2(b), respectively, and are in agreement with the observations made in Refs. [25, 49]. Using the ground state solutions, we calculate the full excitation spectrum of the mixture by solving BdG Eqs. (13) numerically for the Bogoliubov model using a basis expansion method [51]. In the spectrum, there are three zero-energy modes: two of these correspond to the Goldstone modes due to the breaking of $U(1)$ gauge symmetry, while one arises from self-trapping [52]. For the sake of brevity, we have not included the zero-energy modes in the spectrum. These modes also serve as a self-consistency check to verify the accuracy of our numerical calculations. We characterize the density or spin character of the l th excitation mode by a measure Q_l defined as $Q_l = S_-^l/S_+^l$, where $S_{\pm}^l = \int [\{\delta n^l(x)\}^2 \pm \{\delta s^l(x)\}^2] dx$ [53, 54]. Here $\delta n^l(x) = \delta n_1^l(x) + \delta n_2^l(x)$ and $\delta s^l(x) = \delta n_1^l(x) - \delta n_2^l(x)$, where $\delta n_{\nu}^l(x) = \text{Re}[\phi_{\nu}(u_{\nu}^{l*} - v_{\nu}^l)]$ is the density fluctuation

in the component ν generated by the l th Bogoliubov mode.

The excitation spectrum as a function of g_{12}/g for $N = 20$ and $N = 80$ are shown in Figs. 3(a) and 3(b), respectively. With an increase in g_{12} , i.e., an increase in net mean-field repulsion, all the excitation energies monotonically decrease. For $-g < g_{12} \lesssim -0.775g$ for $N = 20$ and $-g < g_{12} \lesssim -0.85g$ for $N = 80$, all the excitations below the particle emission threshold are density excitations with $Q = 1$, the lowest of which is the density breathing mode. For $g_{12} \gtrsim -0.775g$ ($-0.85g$) for $N = 20$ (80), the spin channel is sufficiently softened, leading to the appearance of spin excitations below the particle emission threshold with $Q = -1$. Similar to the density channel, the lowest lying spin excitation is the (spin) breathing mode. We also examine the excitation spectrum as a function of N for fixed coupling strengths [see Figs. 3(c) for $g_{12} = -0.6g$ and 3(d) for $g_{12} = -0.5g$]. Here, too, there is a monotonic decrease in excitation energies with more spin excitations appearing below the particle emission threshold as N increases. For $g_{11} = g_{22}$, the den-

sity and spin channels are fully decoupled, as evidenced by the modes with $Q = +1$ or -1 , where the density and spin modes, respectively, correspond to in-phase and out-of-phase modes. This is demonstrated by the quasiparticle amplitudes

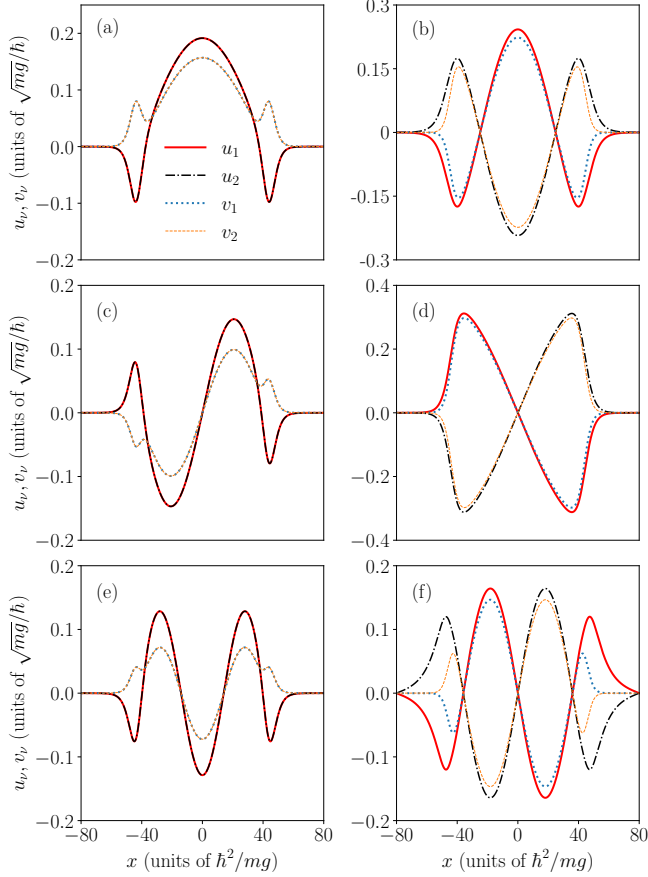


FIG. 4. The quasiparticle amplitudes of the three lowest lying density and spin modes for $N = 60$ and $g_{12} = -0.6g$ [see Fig. 2(c)]. Left panel: (a) first, (c) second and, (e) third density mode. Right panel: (b) first, (d) second, and (f) third spin mode. Density modes correspond to in-phase oscillations with $u_1 = u_2$ and $v_1 = v_2$, whereas spin modes correspond to out-of-phase oscillations with $u_1 = -u_2$ and $v_1 = -v_2$.

(u_ν, v_ν) of the three lowest lying density modes in the left panel of Fig. 4 and spin modes in the right panel of Fig. 4 for $g_{12} = -0.6$ and $N = 60$; density modes have $u_1 = u_2$ and $v_1 = v_2$, whereas for spin modes $u_1 = -u_2$ and $v_1 = -v_2$. For $g_{11} = g_{22}$, $\mathcal{R}(\zeta)$ monotonically decreases from $4/3$ to $2\sqrt{2}/3$ as g_{12} increases from $-g$ to 0 [49]. This effectively reduces the strength of the attractive LHY correction, resulting in flatter droplets within Bogoliubov theory vis-à-vis Petrov's. We find that excitation energies within Bogoliubov theory are perceptibly lower than those obtained in Petrov's theory. This is illustrated by the density and spin breathing modes calculated for the two models and plotted as a function of g_{12} and N in Figs. 5(a) and 5(b).

Variational Analysis:— To further understand the density and spin breathing modes, we consider the variational ansatz

given by

$$\phi_\nu(x, t) = \sqrt{\frac{N}{2\sqrt{\pi}\sigma_\nu(t)}} \exp\left[-\frac{x^2}{2\sigma_\nu(t)^2} + i\beta_\nu(t)x^2\right], \quad (23)$$

where $\sigma_\nu(t)$ and $\beta_\nu(t)$, which denote the width of the self-bound solution and the chirp, respectively, are the time-dependent variational parameters. The Lagrangian of the system is

$$L = \int dx \sum_\nu \frac{i}{2} \left(\phi_\nu^* \frac{\partial \phi_\nu}{\partial t} - \phi_\nu \frac{\partial \phi_\nu^*}{\partial t} \right) - E, \quad (24a)$$

$$= L_K + L_{MF} + L_{LHY}, \quad (24b)$$

where E is the energy of the system and L_K, L_{MF} , and L_{LHY} are the contributions of the kinetic energy, mean field, and beyond mean field interactions to the Lagrangian. Using Eqs. (23) and (24), the first two contributions to the Lagrangian are

$$L_K = -\frac{N}{4} \sum_{\nu=1,2} \left(\sigma_\nu^2 \dot{\beta}_\nu + 2\sigma_\nu^2 \beta_\nu^2 + \frac{1}{2\sigma_\nu^2} \right), \quad (25)$$

$$L_{MF} = -\frac{N^2}{16\sqrt{\pi}} \left(\frac{\sqrt{2}g(\sigma_1 + \sigma_2)}{\sigma_1\sigma_2} + \frac{4g_{12}}{\sqrt{\sigma_1^2 + \sigma_2^2}} \right). \quad (26)$$

The LHY contribution to the Lagrangian reads as

$$L_{LHY} = \int dx \frac{g^{3/2}}{2} \left(\sum_{\nu=1,2} |\phi_\nu|^2 \right)^{3/2} \mathcal{R}(p). \quad (27)$$

To make it analytically tractable, we express widths as $\sigma_1(t) = [\sigma_1(t) + \sigma_2(t)]/2 + [\sigma_1(t) - \sigma_2(t)]/2$ and $\sigma_2(t) = [\sigma_1(t) + \sigma_2(t)]/2 - [\sigma_1(t) - \sigma_2(t)]/2$ and Taylor series expand the integrand about the mean instantaneous width $[\sigma_1(t) + \sigma_2(t)]/2$ up to the second order in $[\sigma_1(t) - \sigma_2(t)]/2$. The estimate of L_{LHY} thus obtained is

$$L_{LHY} = -\frac{g^{3/2}N^{3/2}}{864\sqrt{6}\pi^{5/4}(\sigma_1 + \sigma_2)^{9/2}} \times \left[576\mathcal{C}_1(\sigma_1 + \sigma_2)^4 + 432\mathcal{C}_2(\sigma_1^2 - \sigma_2^2)^2 + \frac{\mathcal{C}_3}{16}(\sigma_1 - \sigma_2)^4 \right], \quad (28)$$

where $\mathcal{C}_1, \mathcal{C}_2$, and \mathcal{C}_3 are defined in Eqs. (46a)-(46c) in the Appendix. Using the Lagrangian, we write the Euler-Lagrange equations for $\beta_\nu(t)$, which are $\beta_\nu(t) = \dot{\sigma}_\nu(t)/2\sigma_\nu(t)$, along with $\sigma_\nu(t)$ [see Eq. (47) in the Appendix]. We linearize the two coupled Euler-Lagrange equations for variables $\sigma_\nu(t)$ about the equilibrium widths $\sigma_1^{\text{eq}} = \sigma_2^{\text{eq}} = \sigma$ to arrive at the coupled equations for fluctuations in widths about the equilibrium value

$$\delta\ddot{\sigma}_1(t) + \omega_{11}^2\delta\sigma_1(t) + \omega_{12}^2\delta\sigma_2(t) = 0, \quad (29a)$$

$$\delta\ddot{\sigma}_2(t) + \omega_{21}^2\delta\sigma_1(t) + \omega_{22}^2\delta\sigma_2(t) = 0, \quad (29b)$$

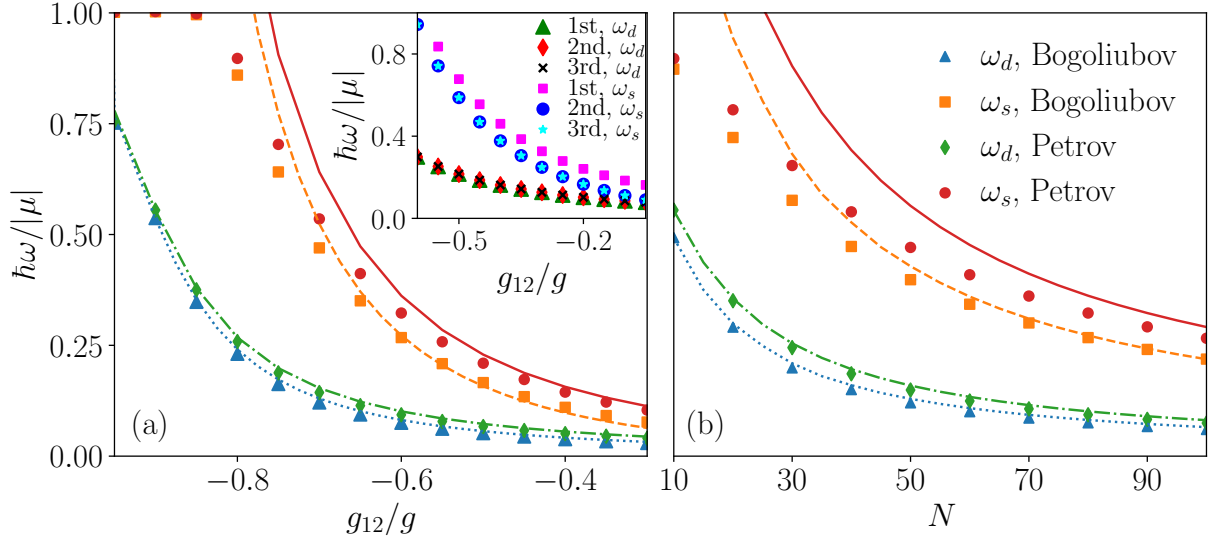


FIG. 5. Comparison of density- and spin-breathing mode energies obtained from Petrov's and Bogoliubov's models. (a) Excitation energies as a function of g_{12}/g for $N = 80$. (b) Excitation energies as a function of N for $g_{12}/g = -0.6g$. Numerical BdG results are shown together with variational calculations (continuous lines in matching colors). The blue dotted (green dash-dotted) curve denotes the density-breathing mode obtained from the Bogoliubov (Petrov) model, while the orange dashed (red solid) curve corresponds to the spin-breathing mode from the Bogoliubov (Petrov) model. Inset in (a): comparison of variational results for $N = 20$ within the Bogoliubov model, where the LHY term is expanded up to first, second, and third order in $(\sigma_1(t) - \sigma_2(t))/2$.

where $\omega_{11}^2 = \omega_{22}^2 = \omega_1^2$ and $\omega_{12}^2 = \omega_{21}^2 = \omega_2^2$. The equilibrium width σ satisfies

$$\frac{1}{\sigma^3} + \frac{N(g + g_{12})}{2\sqrt{2\pi}\sigma^2} - \frac{\sqrt{N}g^{3/2}}{3\sqrt{3}\pi^{5/4}\sigma^{3/2}} \times \left[(1 + |\gamma|)^{3/2} - \frac{\eta(|\gamma| - 1)}{\sqrt{1 + |\gamma|}} \right] = 0, \quad (30)$$

where $\gamma = g_{12}/g$ for Bogoliubov's or -1 for Petrov's model and $\eta = \sqrt{1 - \gamma^2}$. The ω_1^2 and ω_2^2 have the following forms

$$\omega_1^2 = \frac{3}{\sigma^4} + \frac{gN(4 + \gamma)}{4\sqrt{2\pi}\sigma^3} + \frac{\sqrt{3N}g^{3/2}}{12\pi^{5/4}\sigma^{5/2}|\gamma|\sqrt{1 + |\gamma|}} \times \left[(1 + |\gamma|)^2(|\gamma| - 2) - \eta(|\gamma| - 1)(|\gamma| + 2) \right], \quad (31a)$$

$$\omega_2^2 = \frac{3Ng_{12}}{4\sqrt{2\pi}\sigma^3} - \frac{\sqrt{3N}g^{3/2}}{12\pi^{5/4}\sigma^{5/2}|\gamma|\sqrt{1 + |\gamma|}} \times \left[(1 + |\gamma|)^2(3|\gamma| - 2) - \eta(|\gamma| - 1)(3|\gamma| + 2) \right]. \quad (31b)$$

Using $\delta\sigma_1(t) = \delta\sigma_2(t)$ for the density breathing and $\delta\sigma_1(t) = -\delta\sigma_2(t)$ for spin breathing mode in Eqs. (29), the frequencies of the density-breathing mode (ω_d) and spin-breathing mode (ω_s) are $\omega_d^2 = (\omega_1^2 + \omega_2^2)$ and $\omega_s^2 = (\omega_1^2 - \omega_2^2)$. The variational estimates of density and spin breathing modes are in good agreement with the numerical results, especially for larger number of bosons [see Figs. 5(a) and (b)].

We confirmed that the Taylor series expansion up to second

order in $\epsilon(t) = [\sigma_1(t) - \sigma_2(t)]/2$ is sufficient to approximate the integrand in (27), as the inclusion of higher order terms does not lead to any perceptible changes. This can be seen in the inset of Fig. 5(a), showing the variationally calculated frequencies of the breathing modes (for the Bogoliubov model) as a function of g_{12} for $N = 20$ using linear, quadratic, and cubic polynomial approximations to the integrand.

IV. SCALAR BOSE-BOSE MIXTURE

We now study a scalar Bose-Bose mixture in which the number of atoms in each species, N_ν , is independently fixed. To examine the excitation spectrum as a function of particle imbalance $\delta N = N_1 - N_2$, we consider the mixture with equal intraspecies coupling strengths ($g_{11} = g_{22} = g$) and $g_{12} = -0.8g$. In Fig. 6, we show the densities of two components for different δN with $N = 100$. The densities are symmetrical about $x = 0$ for all δN . For $N_1 = N_2$, the densities of the two components overlap as shown in Fig. 6 (a). As δN is increased, the difference in the peak densities at $x = 0$ increases for small particle imbalances [see Figs. 6(a)-(c)]. The additional atoms are accommodated by the droplet without any significant increase in the root mean square (rms) sizes of the two components for $\delta N < 8$. On a further increase in δN , the difference in the peak densities and the rms size of the minority component do not change much, whereas the rms size of the majority component grows exponentially due to the excess (unbound) atoms sandwiching the droplet. The densities for $\delta N = 10$ and $\delta N = 14$ are shown in Figs. 6(d) and (e). The variation in the peak density differ-

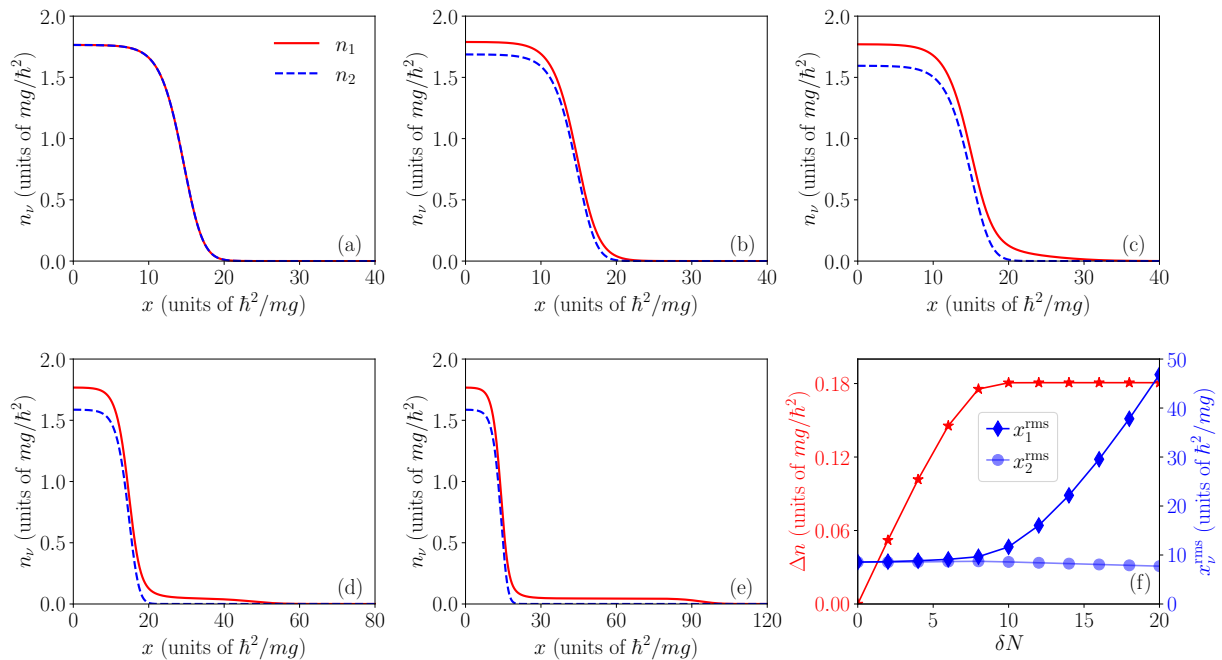


FIG. 6. Density profiles of scalar mixtures with $g_{12} = -0.8g$ and $N = 100$ for (a) $\delta N = 0$, (b) $\delta N = 4$, (c) $\delta N = 8$, (d) $\delta N = 10$, and (e) $\delta N = 14$. (f) shows the difference in the densities of the two components at $x = 0$, $\Delta n = n_1(x = 0) - n_2(x = 0)$, and the rms sizes of the components, x_ν^{rms} , as a function of δN .

ence, $n_1(x = 0) - n_2(x = 0)$, and the rms sizes of the components x_ν^{rms} as a function of δN are shown in Fig. 6(f). Similar changes in the ground-state features have been observed in recently studied particle-imbalanced 3D quantum droplets [22, 23].

We first study the breathing oscillations of imbalanced droplets by tracking the real-time evolution of ground states generated by a perturbed Hamiltonian. More precisely, we perturb the intraspecies coupling g by changing it to $1.001g$ at $t = 0$ and examine the oscillations in mean-square sizes, $\langle x^2 \rangle_\nu(t) = \int x^2 |\Phi_\nu(x, t)|^2 dx / N_\nu$, of the two components. For $\delta N < 8$, $\langle x^2 \rangle_\nu(t)$ oscillate with a single frequency, as shown in Figs. 7 (a)-(d) for $\delta N = 4$. This represents the density breathing mode of the droplet. For $\delta N \geq 8$, $\langle x^2 \rangle_1(t)$ oscillates with a distinctive beat pattern in contrast to $\langle x^2 \rangle_2(t)$ as is seen in Figs. 7 (e) and (g) for $\delta N = 10$. The Fourier transform of $\langle x^2 \rangle_\nu(t)$ [see Figs. 7 (f) and (h)] confirms two frequencies in $\langle x^2 \rangle_1(t)$, the larger of which matches the oscillation frequency of the minority component. The ground state solution for $\delta N \geq 8$ has two distinct regions: an overlap or core region corresponding to the self-bound droplet and an outer region corresponding to the halo of the majority component's atoms. This suggests that the beat pattern in the oscillations of $\langle x^2 \rangle_1(t)$ may correspond to two different length scales, corresponding to the size of the core or droplet proper and the majority component's overall size, which includes the outer unbound gas in which the droplet now lies immersed. To shed more light on this, we approximate the overlap extent of two components by the rms size of the minority component

$x_2^{\text{rms}} = \sqrt{\langle x^2 \rangle_2(t = 0)}$ and split $\langle x^2 \rangle_1(t)$ as

$$\langle x^2 \rangle_1(t) = \frac{1}{N_1} \left[\int_{-x_2^{\text{rms}}}^{x_2^{\text{rms}}} x^2 |\Phi_1(x, t)|^2 dx + \int_{-\infty}^{-x_2^{\text{rms}}} x^2 |\Phi_1(x, t)|^2 dx + \int_{x_2^{\text{rms}}}^{\infty} x^2 |\Phi_1(x, t)|^2 dx \right]. \quad (32)$$

The first term on the right hand side of Eq. (32) corresponds to the overlap region and is plotted in Fig. 8(a) and its Fourier transform in Fig. 8(b), showing that it oscillates with two frequencies with smaller of the two matches the oscillation frequency of the minority component, and the other corresponds to the chemical potential of the minority component. We identify the smaller frequency to be associated with the density breathing mode of the droplet for $\delta N \geq 8$. The oscillations in the other two terms plotted in Fig. 8(c) and its Fourier transform in Fig. 8(d) contain three frequencies, two of which match the oscillations in $\langle x^2 \rangle_1(t)$ in Fig. 7(e) and a third, largest of the three frequencies, corresponds to the chemical potential of the minority component.

In Fig. 9 (a), we plot the negative of the chemical potentials of two components and the density breathing mode frequency as functions of particle imbalance. With an increase in δN , absolute value of chemical potential of the minority (majority) component increases (decreases) till $\delta N < 8$, beyond which the chemical potentials μ_ν do not change. The density breathing mode is below the particle emission thresholds for both components for $\delta N < 8$, whereas for $\delta N \geq 8$,

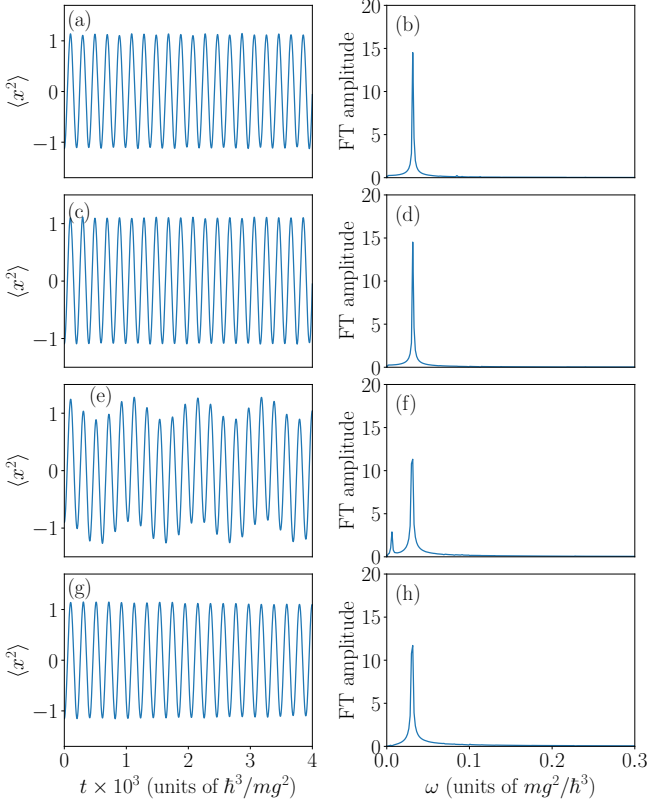


FIG. 7. (a) and (c) show the temporal oscillations in the mean square sizes, $\langle x^2 \rangle_\nu = \int x^2 |\Phi_\nu(x, t)|^2 dx / N_\nu$, of major ($\nu = 1$) and minor ($\nu = 2$) components, respectively, centered around zero by subtracting their equilibrium mean values, with particle imbalance $\delta N = 4$ and $g_{12} = -0.8g$; the amplitudes of their corresponding Fourier transforms (FT) are shown in (b) and (d). (e) and (g) show the oscillations in $\langle x^2 \rangle_\nu$ for major and minor components respectively, with particle imbalance $\delta N = 10$ alongside their respective Fourier transforms in (f) and (h). $\langle x^2 \rangle_\nu$ is measured in units of \hbar^4/m^2g^2 .

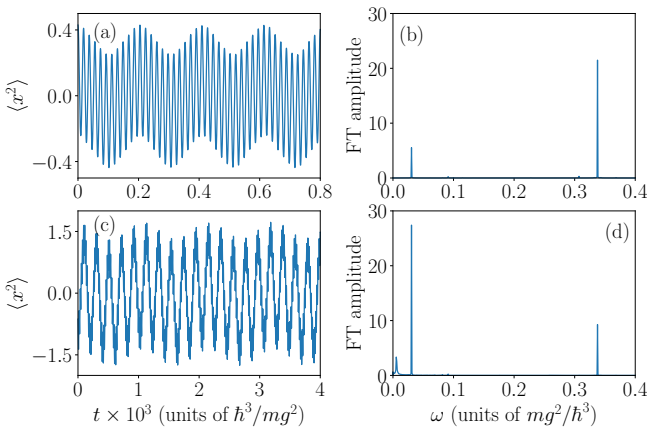


FIG. 8. (a) shows the mean-subtracted temporal oscillations of the first term on the right-hand side of Eq. (32), for $\delta N = 10, g_{12} = -0.8$ with the amplitude of its Fourier transform (FT) in (b). The identical oscillations of the other two terms in Eq. (32) are shown in (c), and its Fourier transform in (d)

the density breathing mode's frequency becomes larger than the particle emission threshold for the majority component. Similar observations have been made for particle imbalanced 3D droplets [22, 23]. We further calculated the complete excitation spectrum of the mixture as a function of δN by solving BdG Eqs. (13). From the spectrum shown in Fig. 9(b), we find that for $\delta N < 8$, the density breathing mode with $Q = 1$ decreases with increasing population imbalance and is the lowest lying non-zero energy excitation with the same frequency as identified from the real-time dynamics. The situation is drastically different for $\delta N \geq 8$ when there are many non-zero excitations all below the particle emission threshold of the majority component, i.e., with $\omega < |\mu_1|$. The density mode gradually hardens as δN is increased, with its frequency matching with the results from the real-time dynamics. The lowest non-zero frequency matches with the smaller of the two frequencies in the oscillations of $\langle x^2 \rangle_1(t)$ for $\delta N \geq 8$ [see Figs. 7 (e) and (f)]. The spectrum shown in Fig. 9(b), therefore, validates the real-time dynamics and the identification of the density breathing mode in the previous paragraph.

Variational Analysis:— To further vindicate the role of two length scales on the breathing dynamics of the system, we construct a variational analysis. We consider the variational ansatz given by

$$\begin{aligned} \phi_1(x, t) &= \begin{cases} \phi_1^{\text{out}}(x, t), & |x| \gtrsim 3\sigma_2(t) \\ \phi_1^{\text{in}}(x, t), & |x| \lesssim 3\sigma_2(t) \end{cases} \\ &= \begin{cases} A_1 \sqrt{\frac{N_1}{\sqrt{\pi}\sigma_1(t)}} e^{\left[-\frac{x^2}{2\sigma_1(t)^2} + i\beta_1(t)x^2\right]}, & |x| \gtrsim 3\sigma_2(t) \\ A_2 \sqrt{\frac{N_1}{\sqrt{\pi}\sigma_2(t)}} e^{\left[-\frac{x^2}{2\sigma_2(t)^2} + i\beta_2(t)x^2\right]}, & |x| \lesssim 3\sigma_2(t) \end{cases} \end{aligned} \quad (33a)$$

$$\phi_2(x, t) = \sqrt{\frac{N_2}{\sqrt{\pi}\sigma_2(t)}} \exp\left[-\frac{x^2}{2\sigma_2(t)^2} + i\beta_2(t)x^2\right], \quad (33b)$$

where $\sigma_2(t)$ is a measure of the size of the overlap region or of the self-bound droplet, and $\sigma_1(t)$ is the overall size of the majority component, including the outer “shell” of the unbound gas consisting solely of atoms of the majority component. We assume that $\sigma_1(t) \gg \sigma_2(t)$ to make the integrals in the Lagrangian (24) tractable; for example, L_{LHY} in Eq. (27) can be approximated as

$$\begin{aligned} L_{\text{LHY}} &= \int_{-\infty}^{\infty} \mathcal{L}(\phi_1, \phi_2) dx, \\ &\approx \int_{-\infty}^{\infty} \mathcal{L}(\phi_1^{\text{in}}, \phi_2) dx + \int_{-\infty}^{\infty} \mathcal{L}(\phi_1^{\text{out}}, \phi_2 \approx 0) dx. \end{aligned} \quad (34)$$

The Euler-Lagrange equations for $\sigma_1(t)$ and $\sigma_2(t)$ thus ob-

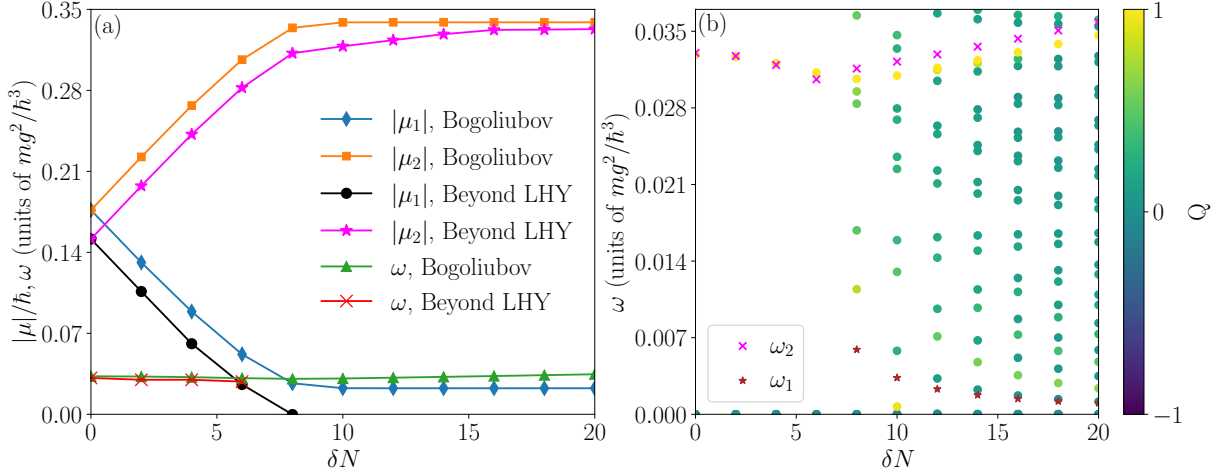


FIG. 9. (a) $|\mu_1|/\hbar$, $|\mu_2|/\hbar$, and the frequency of the density breathing mode (ω) as a function of $\delta N = N_1 - N_2$ of a scalar mixture with $N = 100$ and $g_{12} = -0.8g$. For $\delta N \geq 8$, the Bogoliubov theory leads to the density breathing mode's energy exceeding $|\mu_1|$. The beyond-LHY theory leads to reduced $|\mu_\nu|$ with $|\mu_1| \approx 0$ for $\delta N \geq 8$. (b) The low-lying excitation energies of the scalar mixture with $N = 100$ and $g_{12} = -0.8g$ along with variational estimates ω_1 and ω_2 (density-breathing mode) as given in Eqs. (36a) and (36b).

tained are

$$\ddot{\sigma}_1 = \frac{1}{\sigma_1^3} - \frac{(A_2^2 - 1)gN_1}{\sqrt{2\pi}\sigma_1^2} - \frac{2\sqrt{2}g^{3/2}\sqrt{(1 - A_2^2)N_1}}{3\sqrt{3}\pi^{5/4}\sigma_1^{3/2}}, \quad (35a)$$

$$\ddot{\sigma}_2 = \frac{1}{\sigma_2^3} + \frac{1}{\sqrt{2\pi}\sigma_2^2} \left[g\tilde{N} - \frac{2A_2^2N_1N_2(g - g_{12})}{\tilde{N}} \right] - \frac{g^{3/2}\sqrt{\tilde{N}}}{3\sqrt{3}\pi^{5/4}\sigma_2^{3/2}} \left[(1 - \sqrt{1 - \Lambda})^{3/2} + (1 + \sqrt{1 - \Lambda})^{3/2} \right], \quad (35b)$$

where $\tilde{N} = A_2^2N_1 + N_2$ is the variational estimate of effective total particle number in the droplet, and $\Lambda = 4A_2^2N_1N_2\eta^2/\tilde{N}^2$. Linearization of the Euler-Lagrange equations yields $\delta\ddot{\sigma}_\nu(t) + \omega_\nu^2\delta\sigma_\nu(t) = 0$ with

$$\omega_1^2 = \frac{3}{\sigma_1^4} - \sqrt{\frac{2}{\pi}} \frac{(A_2^2 - 1)gN_1}{\sigma_1^3} - \sqrt{\frac{2}{3}} \frac{g^{3/2}\sqrt{(1 - A_2^2)N_1}}{\pi^{5/4}\sigma_1^{5/2}}, \quad (36a)$$

$$\omega_2^2 = \frac{3}{\sigma_2^4} + \sqrt{\frac{2}{\pi}} \frac{1}{\sigma_2^3} \left[g\tilde{N} - \frac{2A_2^2N_1N_2(g - g_{12})}{\tilde{N}} \right] - \frac{g^{3/2}\sqrt{\tilde{N}}}{2\sqrt{3}\pi^{5/4}\sigma_2^{5/2}} \left[(1 - \sqrt{1 - \Lambda})^{3/2} + (1 + \sqrt{1 - \Lambda})^{3/2} \right], \quad (36b)$$

where σ_1 and σ_2 are the equilibrium measures. These, along with A_2 , are fixed by minimizing the ground-state variational

energy

$$E_0 = \frac{N_1(1 - A_2^2)}{4\sigma_1^2} + \frac{\tilde{N}}{4\sigma_2^2} + \frac{g(1 - A_2^2)^2N_1^2}{2\sqrt{2\pi}\sigma_1} + \frac{[g\tilde{N}^2 - 2A_2^2N_1N_2(g - g_{12})]}{2\sqrt{2\pi}\sigma_2} - \frac{2\sqrt{2}[gN_1(1 - A_2^2)]^{3/2}}{3\sqrt{3}\pi^{5/4}\sqrt{\sigma_1}} - \frac{(g\tilde{N})^{3/2}}{3\sqrt{3}\pi^{5/4}\sqrt{\sigma_2}} \left[(1 - \sqrt{1 - \Lambda})^{3/2} + (1 + \sqrt{1 - \Lambda})^{3/2} \right]. \quad (37)$$

Eqs. (36a)-(37) describe the variational estimates for $\delta N \geq 8$.

For $\delta N < 8$, all the atoms of the majority component are bound within the droplet. In this case, we set $A_1 = 0$ and $A_2 = 1$, so the Lagrangian's dependence on ϕ_1^{out} [or $\sigma_1(t)$, $\beta_1(t)$ and their derivatives] drops out. The equation of motion of the droplet's size $\sigma_2(t)$ is again given by Eq. (35b) and density breathing mode frequency by ω_2 in Eq. (36b). The variational results for ω_1 and ω_2 are shown in Fig. 9(b) and are in good agreement with the corresponding modes in the BdG spectrum.

V. SELF-BOUND DROPLET TO UNBOUND GAS TRANSITION

The Bogoliubov theory supports the droplet phase across the entire mean-field stability regime [49]. The validity of the theory requires that $n|a_{\nu\nu'}| \gg 1$ and since the peak density decreases with an increase in δg before getting saturated, the theory's validity is not guaranteed across the entire mean-field stability regime. Furthermore, quantum Monte Carlo studies have shown that there is a liquid to unbound gas transition for $g_{12} > -0.46$ in a pseudospinor 1D Bose-Bose mixture [47, 48].

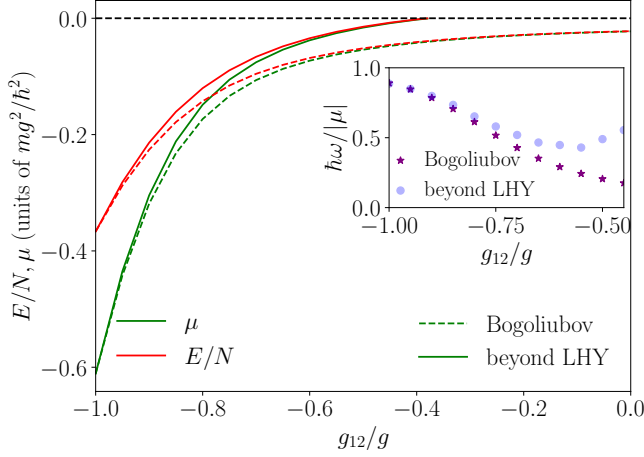


FIG. 10. Comparison of the energy per particle and chemical potential obtained from the Bogoliubov and the beyond LHY theory for pseudospinor mixture with $N = 20$. The inset shows the energy of the density-breathing mode, scaled by the chemical potential, for these two theories.

In this subsection, we implement a beyond LHY description of Bose-Bose mixtures [16], using beyond mean field expressions for sound velocities in Eq. (5), to validate the regimes studied in this work and to re-examine the density breathing mode. We again consider $g_{11} = g_{22} = g$, which sets the

equilibrium density difference to zero for a pseudospinor mixture, but not for a scalar mixture with population imbalance ($\delta N > 0$) [see Fig. 6(f)]. To obtain the beyond-mean-field expressions for sound velocities applicable for both these systems, we first calculate the compressibility (κ_-) and susceptibility (κ_+) using [16]

$$\kappa_- = \frac{1}{n^2} \left(\frac{\partial^2 \mathcal{E}}{\partial n^2} \right)^{-1}, \quad \kappa_+ = \frac{1}{n^2} \left(\frac{\partial^2 \mathcal{E}}{\partial (\Delta n)^2} \right)^{-1}, \quad (38)$$

where \mathcal{E} is energy density (1) and $n = n_1 + n_2$ and $\Delta n = n_1 - n_2$. Then using $c_{\pm} = \sqrt{1/(n\kappa_{\pm})}$, we obtain the following beyond mean-field expressions for sound velocities and their respective derivatives

$$c_+^2 = \frac{n(g - g_{12})}{2} - \frac{g\eta^2 \sqrt{2gmn}}{8\hbar\pi} \left(\frac{\Delta n^2 \eta^2 \mathcal{Q}}{n^2(p+1)} - 4\sqrt{2} \left(\frac{\Delta n^2 \eta^2}{n^2(p+1)} - 1 \right) \frac{\partial \mathcal{R}}{\partial p} \right), \quad (39a)$$

$$c_-^2 = \frac{n(g + g_{12})}{2} - \frac{g\sqrt{2gmn}}{8\hbar\pi(p+1)} \left((1+p+\gamma^4)\mathcal{Q} + 4\sqrt{2}\gamma^2 \left(\frac{\Delta n^2 \eta^2}{n^2} - \frac{p+1}{\sqrt{-p}} \right) \frac{\partial \mathcal{R}}{\partial p} \right), \quad (39b)$$

$$\frac{\partial c_+^2}{\partial n_{\nu}} = \frac{(g - g_{12})}{2} - \frac{g\eta^2 \sqrt{2gmn}}{8\hbar\pi} \left[\frac{\Delta n^2 \eta^2 \mathcal{Q}}{2n^3(p+1)} + \frac{2\mathcal{Q}\eta^2 \Delta n}{n^2(p+1)} \left(s_{\nu} - \frac{\Delta n}{n} \right) + \frac{\Delta n^2 \eta^2}{n^2(p+1)} \frac{\partial p}{\partial n_{\nu}} \left(\frac{\partial \mathcal{Q}}{\partial p} - \frac{\mathcal{Q}}{1+p} \right) - \frac{4\sqrt{2}\Delta n\eta^2}{n^2(p+1)} \frac{\partial \mathcal{R}}{\partial p} \left(2(-1)^{\nu+1} - \frac{2\Delta n}{n} - \frac{\Delta n}{p+1} \frac{\partial p}{\partial n_{\nu}} \right) - 2\sqrt{2} \left(\frac{\Delta n^2 \eta^2}{n^2(p+1)} - 1 \right) \left(\frac{1}{n} \frac{\partial \mathcal{R}}{\partial p} + 2 \frac{\partial^2 \mathcal{R}}{\partial p^2} \frac{\partial p}{\partial n_{\nu}} \right) \right], \quad (40a)$$

$$\frac{\partial c_-^2}{\partial n_{\nu}} = \frac{(g + g_{12})}{2} - \frac{g\sqrt{2gmn}}{8\hbar\pi(p+1)} \left[\left(\frac{1}{2n} - \frac{1}{p+1} \frac{\partial p}{\partial n_{\nu}} \right) (1+p+\gamma^4)\mathcal{Q} + \left(\mathcal{Q} + (1+p+\gamma^4) \frac{\partial \mathcal{Q}}{\partial p} \right) \frac{\partial p}{\partial n_{\nu}} + 4\sqrt{2}\gamma^2 \left(\frac{\Delta n^2 \eta^2}{n^2} - \frac{p+1}{\sqrt{-p}} \right) \left(\frac{\partial^2 \mathcal{R}}{\partial p^2} \frac{\partial p}{\partial n_{\nu}} + \frac{\partial \mathcal{R}}{\partial p} \left(\frac{1}{2n} - \frac{1}{p+1} \frac{\partial p}{\partial n_{\nu}} \right) \right) + 4\sqrt{2}\gamma^2 \frac{\partial \mathcal{R}}{\partial p} \left(\frac{2\Delta n\eta^2}{n^2} \left(s_{\nu} - \frac{\Delta n}{n} \right) - \frac{1}{\sqrt{-p}} \frac{\partial p}{\partial n_{\nu}} \left(1 - \frac{p+1}{2p} \right) \right) \right] \quad (40b)$$

where $s_{\nu} = (-1)^{\nu+1}$ and

$$p = \frac{4(g_{12}^2 - g^2)n_1 n_2}{g^2 n^2}, \quad (41a)$$

$$\mathcal{Q}(p) = \frac{1}{\sqrt{1 - \sqrt{p+1}}} + \frac{1}{\sqrt{1 + \sqrt{p+1}}}, \quad (41b)$$

and $\mathcal{R}(p)$ is defined in Eq. (7b). The beyond-mean field sound velocities c_{\pm} in Eqs. (39a) and (39b) are substituted in Eqs. (1) to obtain the beyond-Bogoliubov expression for the energy density. Similarly, Eq. (5) along with Eqs. (39) and (40) pro-

vide the beyond-LHY correction term appearing in the GP Eq. (4).

The beyond LHY description results in a liquid-to-gas transition at $g_{12} \approx -0.38g$ for pseudospinor mixture [16]. This is illustrated in Fig. 10, where the ground state energy per particle and the chemical potential are plotted as functions of g_{12}/g at $N = 20$ using the Bogoliubov theory and the beyond LHY description. We can see that at $g_{12} \approx -0.38g$, E/N and μ calculated using beyond LHY approach 0, and after that the droplet is no longer self-bound. But in Bogoliubov theory, E/N and μ are negative even for $g_{12} > -0.38g$ and

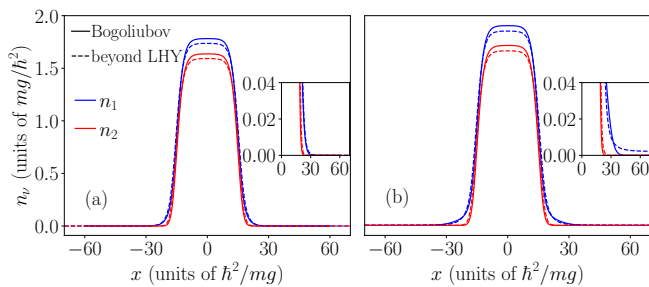


FIG. 11. The density profiles compare the Bogoliubov and the beyond LHY theories at two different values of δN : (a) $\delta N = 6$ and (b) $\delta N = 8$. The insets provide a closer view of the behaviour near the edges of the droplet. At $\delta N = 6$, both models exhibit vanishing densities near the edges. However, at $\delta N = 8$, the Bogoliubov model still predicts vanishing densities for both components near the edges; the beyond-LHY model gives a finite edge density for the majority component, which ends up occupying the entire 1D box size considered in the simulation, and zero density for the minority component.

the droplet is still self-bound [16]. We calculate the density-breathing mode from the real-time evolution of the ground state within the beyond-LHY prescription, i.e., using Eqs. (4) with (5) evaluated using the beyond-mean-field estimates of phonon velocities and their derivatives. The inset in Fig. 10 shows the comparison of the density-breathing mode's energies obtained from the Bogoliubov theory and the beyond LHY prescription. Within beyond-LHY formalism, the density breathing mode's energy scaled with respect to particle emission threshold, first decreases with an increase in g_{12}/g , and near the liquid-to-gas transition point, it starts increasing as the particle emission threshold approaches zero.

We also use the beyond LHY description for the scalar mixture discussed in Sec. V. The beyond LHY chemical potentials of the two components are plotted in Fig. 9 (a). The chemical potential of the majority component approaches zero with an increase of particle imbalance, and for $\delta N \geq 8$, $\mu_1 \approx 0$, and we have an unbound gas of the majority component outside the droplet. This is further illustrated in Figs. 11 (a) and (b), showing a comparison of the density profiles of the solutions obtained with the Bogoliubov and the beyond-LHY theories. For $\delta N < 8$, both theories result in localized self-trapped solutions with vanishing densities outside the droplet, as can be seen in the inset of Fig. 11(a) (for $\delta N = 6$). For $\delta N = 8$, beyond-LHY theory results in finite density of the majority component outside the droplet filling up the entire extent of the simulation box, however large, unlike density profile obtained from the Bogoliubov theory, which is still confined within the simulation box [see inset of Fig. 11(b)]. Additionally, we examined the density breathing mode of the system from the real-time evolution of the ground state for $\delta N < 8$ within the beyond-LHY prescription, namely Eqs. (4)

with (5) evaluated using the beyond-mean-field estimates of phonon velocities and their derivatives. The energy of the breathing excitation as a function of δN thus obtained are slightly lower than the corresponding numbers obtained from the Bogoliubov theory as shown in Fig. 9.

VI. SUMMARY AND CONCLUSIONS

We have conducted theoretical and numerical studies of the collective excitations of one-dimensional quantum droplets in pseudospinor and scalar Bose-Bose mixtures. We employed Bogoliubov theory to access both density (in-phase) and spin (out-of-phase) sectors, and computed the excitation spectrum from the numerical solutions of the Bogoliubov-de Gennes equations. Our findings indicate that for droplets realized within the mean-field stability regime, spin modes can soften and fall below the particle-emission threshold, making them observable in the droplet spectrum.

To complement the full BdG calculations, we developed a variational description of the density and spin-breathing modes. We find good agreement between the variational predictions and the full BdG spectrum. Finally, we corroborated the mode analysis by studying the real-time dynamics of the breathing mode.

For imbalanced droplets, we have demonstrated that as the imbalance increases ($\delta N \geq 8$), two distinct length scales emerge. One is associated with the overlap or core region of the self-bound droplet, while the other corresponds to the halo of the unbound atoms of the majority component. We explain how these two length scales govern the droplet's breathing dynamics, demonstrating that the mode frequencies calculated via the BdG formalism are in excellent agreement with both real-time simulations and variational estimates. We have complemented these studies with an investigation of the liquid to gas transition and the density breathing mode, in both pseudospinor and population-imbalanced scalar mixtures, using a beyond-LHY theory.

Note added:— While finalizing this work, we noticed a recent paper by Xiao et al. [55] which investigates ground-state properties and collective excitations of one-dimensional asymmetric quantum droplets. They specifically evaluate spin-dependent collective modes under confinement, providing an interesting parallel to our results for the spin modes of the self-trapped state presented here.

ACKNOWLEDGMENTS

The work of R Gupta is supported by SERB grant CRG/2023/001388.

APPENDIX:

The elements of the BdG matrix in Eq. (13) are

$$\mathcal{M} = -\frac{\hbar^2}{2m} \frac{\partial^2}{\partial x^2} + 2g_{11}|\phi_1|^2 + g_{12}|\phi_2|^2 - \mu_1 + A_{11}, \quad (42a)$$

$$\mathcal{N} = -\frac{\hbar^2}{2m} \frac{\partial^2}{\partial x^2} + 2g_{22}|\phi_2|^2 + g_{21}|\phi_1|^2 - \mu_2 + A_{22}, \quad (42b)$$

where

$$A_{\nu'\nu} = -\frac{g_{\nu\nu}\sqrt{m(g_{11}n_1 + g_{22}n_2)}}{\hbar\pi} \left(\frac{g_{\nu'\nu'}\phi_\nu\phi_{\nu'}^*}{2(g_{11}n_1 + g_{22}n_2)} + \frac{\partial\phi_\nu}{\partial\phi_{\nu'}} \right), \quad (43a)$$

$$B_{\nu'\nu} = -\frac{g_{\nu\nu}\sqrt{m}}{\hbar\pi} \frac{g_{\nu'\nu'}\phi_\nu\phi_{\nu'}}{2(g_{11}n_1 + g_{22}n_2)}, \quad (43b)$$

for Petrov's model, and

$$\begin{aligned} A_{\nu'\nu} = & -\frac{3g_{\nu\nu}\sqrt{m(g_{11}n_1 + g_{22}n_2)}}{4\hbar\pi} \left(\frac{g_{\nu'\nu'}\mathcal{R}\phi_{\nu'}^*\phi_\nu}{2(g_{11}n_1 + g_{22}n_2)} + \phi_{\nu'}^*\phi_\nu \frac{\partial\mathcal{R}}{\partial p} \frac{\partial p}{\partial n_{\nu'}} + \mathcal{R} \frac{\partial\phi_\nu}{\partial\phi_{\nu'}} + \frac{g_{\nu'\nu'}}{g_{\nu\nu}} \phi_{\nu'}^*\phi_\nu \frac{\partial\mathcal{R}}{\partial p} \frac{\partial p}{\partial n_\nu} \right) \\ & - \frac{\sqrt{m(g_{11}n_1 + g_{22}n_2)}^3}{2\hbar\pi} \left(\phi_{\nu'}^*\phi_\nu \frac{\partial^2\mathcal{R}}{\partial p^2} \frac{\partial p}{\partial n_{\nu'}} \frac{\partial p}{\partial n_\nu} + \frac{\partial\mathcal{R}}{\partial p} \frac{\partial^2 p}{\partial n_{\nu'}\partial n_\nu} \phi_{\nu'}^*\phi_\nu + \frac{\partial\mathcal{R}}{\partial p} \frac{\partial p}{\partial n_\nu} \frac{\partial\phi_\nu}{\partial\phi_{\nu'}} \right), \end{aligned} \quad (44a)$$

$$\begin{aligned} B_{\nu'\nu} = & -\frac{3g_{\nu\nu}\sqrt{m(g_{11}n_1 + g_{22}n_2)}}{4\hbar\pi} \left(\frac{g_{\nu'\nu'}\mathcal{R}\phi_{\nu'}\phi_\nu}{2(g_{11}n_1 + g_{22}n_2)} + \phi_{\nu'}\phi_\nu \frac{\partial\mathcal{R}}{\partial p} \frac{\partial p}{\partial n_{\nu'}} + \frac{g_{\nu'\nu'}}{g_{\nu\nu}} \phi_{\nu'}\phi_\nu \frac{\partial\mathcal{R}}{\partial p} \frac{\partial p}{\partial n_\nu} \right) \\ & - \frac{\sqrt{m(g_{11}n_1 + g_{22}n_2)}^3}{2\hbar\pi} \left(\phi_{\nu'}\phi_\nu \frac{\partial^2\mathcal{R}}{\partial p^2} \frac{\partial p}{\partial n_{\nu'}} \frac{\partial p}{\partial n_\nu} + \frac{\partial\mathcal{R}}{\partial p} \frac{\partial^2 p}{\partial n_{\nu'}\partial n_\nu} \phi_{\nu'}\phi_\nu \right), \end{aligned} \quad (44b)$$

for the Bogoliubov model. In Eqs. (44a) and (44b)

$$\frac{\partial^2 p}{\partial n_\nu^2} = \frac{4g_{\nu\nu}n_{\nu'}(g_{11}g_{22} - g_{12}^2)}{(g_{11}n_1 + g_{22}n_2)^3} - \frac{3g_{\nu\nu}}{(g_{11}n_1 + g_{22}n_2)} \frac{\partial p}{\partial n_{\nu'}}, \quad (45a)$$

$$\frac{\partial^2 p}{\partial n_{\nu'}\partial n_\nu} = \frac{4(g_{11}g_{22} - g_{12}^2)(g_{\nu\nu}n_\nu - 2g_{\nu'\nu'}n_{\nu'})}{(g_{11}n_1 + g_{22}n_2)^3} - \frac{3g_{\nu'\nu'}}{(g_{11}n_1 + g_{22}n_2)} \frac{\partial p}{\partial n_\nu} \quad (45b)$$

Coefficients in L_{LHY} and Euler-Lagrange equation for σ_ν

$\mathcal{C}_1, \mathcal{C}_2$ and \mathcal{C}_3 in L_{LHY} (28) are given as

$$\mathcal{C}_1 = \frac{\gamma^2|\gamma|}{\gamma^4(1-|\gamma|)\sqrt{1+|\gamma|}} \left[\gamma^4 + \gamma^2(|\gamma| - |\gamma|\eta - 1) + |\gamma|(2|\gamma|\eta - \eta - 1) \right], \quad (46a)$$

$$\mathcal{C}_2 = \frac{|\gamma|\eta^2}{\gamma^4(1-|\gamma|)\sqrt{1+|\gamma|}} \left[\gamma^4 - \gamma^2(1 + |\gamma|\eta) + |\gamma|^2\eta \right], \quad (46b)$$

$$\begin{aligned} \mathcal{C}_3 = & \frac{1}{\gamma^4(1-|\gamma|)\sqrt{1+|\gamma|}} \left[\gamma^6(6129|\gamma| - 467) - \gamma^2(8464|\gamma| + 1973|\gamma|^2\eta - 5452|\gamma|\eta + 3012) \right. \\ & \left. - \gamma^4(3689|\gamma| + 6129|\gamma|^2\eta - 5662|\gamma|\eta - 3479) + 3012(2|\gamma| + |\gamma|^2\eta - 2|\gamma|\eta) \right]. \end{aligned} \quad (46c)$$

The equation of motion for the variational parameter σ_ν as referred to in the discussion on the variational method for the pseudospinor mixture in Sec. III is

$$\begin{aligned} \ddot{\sigma}_\nu = & \frac{1}{\sigma_\nu^3} + \frac{N}{\sqrt{\pi}\sigma_\nu^2} \left(\frac{g}{2\sqrt{2}} + \frac{g_{12}\sigma_\nu^3}{(\sigma_\nu^2 + \sigma_{\nu'}^2)^{3/2}} \right) + \frac{\sqrt{N}g^{3/2}}{24\sqrt{6}\pi^{5/4}(\sigma_\nu + \sigma_{\nu'})^{9/2}} \\ & \times \left[32(\sigma_\nu + \sigma_{\nu'})^3\mathcal{C}_1 + 24(\sigma_\nu^2 - \sigma_{\nu'}^2)(\sigma_\nu - 9\sigma_{\nu'})\mathcal{C}_2 + \frac{(\sigma_\nu - \sigma_{\nu'})^3(\sigma_\nu - 17\sigma_{\nu'})}{288(\sigma_\nu + \sigma_{\nu'})}\mathcal{C}_3 \right]. \end{aligned} \quad (47)$$

- [1] D. S. Petrov, *Phys. Rev. Lett.* **115**, 155302 (2015).
- [2] C. R. Cabrera, L. Tanzi, J. Sanz, B. Naylor, P. Thomas, P. Cheiney, and L. Tarruell, *Science* **359**, 301 (2018).
- [3] G. Semeghini, G. Ferioli, L. Masi, C. Mazzinghi, L. Wolswijk, F. Minardi, M. Modugno, G. Modugno, M. Inguscio, and M. Fattori, *Phys. Rev. Lett.* **120**, 235301 (2018).
- [4] P. Cheiney, C. R. Cabrera, J. Sanz, B. Naylor, L. Tanzi, and L. Tarruell, *Phys. Rev. Lett.* **120**, 135301 (2018).
- [5] G. Ferioli, G. Semeghini, L. Masi, G. Giusti, G. Modugno, M. Inguscio, A. Galletí, A. Recati, and M. Fattori, *Phys. Rev. Lett.* **122**, 090401 (2019).
- [6] C. D’Errico, A. Burchianti, M. Prevedelli, L. Salasnich, F. Ancilotto, M. Modugno, F. Minardi, and C. Fort, *Phys. Rev. Res.* **1**, 033155 (2019).
- [7] Z. Guo, F. Jia, L. Li, Y. Ma, J. M. Hutson, X. Cui, and D. Wang, *Phys. Rev. Res.* **3**, 033247 (2021).
- [8] L. Cavicchioli, C. Fort, F. Ancilotto, M. Modugno, F. Minardi, and A. Burchianti, *Phys. Rev. Lett.* **134**, 093401 (2025).
- [9] H. Kadau, M. Schmitt, M. Wenzel, C. Wink, T. Maier, I. Ferrier-Barbut, and T. Pfau, *Nature* **530**, 194 (2016).
- [10] I. Ferrier-Barbut, H. Kadau, M. Schmitt, M. Wenzel, and T. Pfau, *Phys. Rev. Lett.* **116**, 215301 (2016).
- [11] M. Schmitt, M. Wenzel, F. Böttcher, I. Ferrier-Barbut, and T. Pfau, *Nature* **539**, 259 (2016).
- [12] L. Chomaz, S. Baier, D. Petter, M. J. Mark, F. Wächtler, L. Santos, and F. Ferlaino, *Phys. Rev. X* **6**, 041039 (2016).
- [13] D. S. Petrov, (2023), arXiv:2312.05336 [cond-mat.quant-gas].
- [14] C. J. Pethick and H. Smith, *Bose–Einstein Condensation in Dilute Gases* (Cambridge University Press, 2008).
- [15] L. Pitaevskii and S. Stringari, *Bose-Einstein condensation and superfluidity*, Vol. 164 (Oxford University Press, 2016).
- [16] M. Ota and G. E. Astrakharchik, *SciPost Phys.* **9**, 020 (2020).
- [17] H. Hu and X.-J. Liu, *Phys. Rev. Lett.* **125**, 195302 (2020).
- [18] H. Hu, J. Wang, and X.-J. Liu, *Phys. Rev. A* **102**, 043301 (2020).
- [19] Q. Gu and L. Yin, *Phys. Rev. B* **102**, 220503 (2020).
- [20] V. Cikojević, L. V. c. v. Markić, G. E. Astrakharchik, and J. Boronat, *Phys. Rev. A* **99**, 023618 (2019).
- [21] H. Hu and X.-J. Liu, *Phys. Rev. A* **102**, 053303 (2020).
- [22] T. A. Flynn, L. Parisi, T. P. Billam, and N. G. Parker, *Phys. Rev. Res.* **5**, 033167 (2023).
- [23] T. A. Flynn, N. A. Keepfer, N. G. Parker, and T. P. Billam, *Phys. Rev. Res.* **6**, 013209 (2024).
- [24] A. Cappellaro, T. Macrì, and L. Salasnich, *Phys. Rev. A* **97**, 053623 (2018).
- [25] D. S. Petrov and G. E. Astrakharchik, *Phys. Rev. Lett.* **117**, 100401 (2016).
- [26] Y. Li, Z. Chen, Z. Luo, C. Huang, H. Tan, W. Pang, and B. A. Malomed, *Phys. Rev. A* **98**, 063602 (2018).
- [27] M. N. Tengstrand, P. Stürmer, E. O. Karabulut, and S. M. Reimann, *Phys. Rev. Lett.* **123**, 160405 (2019).
- [28] T. A. Yoğurt, U. Tanyeri, A. Keleş, and M. O. Oktel, *Phys. Rev. A* **108**, 033315 (2023).
- [29] G. Bougas, G. C. Katsimiga, P. G. Kevrekidis, and S. I. Mistakidis, *Phys. Rev. A* **110**, 033317 (2024).
- [30] S. R. Otajonov, E. N. Tsoy, and F. K. Abdullaev, *Phys. Rev. A* **106**, 033309 (2022).
- [31] P. Stürmer, M. N. Tengstrand, R. Sachdeva, and S. M. Reimann, *Phys. Rev. A* **103**, 053302 (2021).
- [32] L. Dong, K. Shi, and C. Huang, *Phys. Rev. A* **106**, 053303 (2022).
- [33] Y. Fei, X. Du, X.-L. Chen, and Y. Zhang, *Phys. Rev. A* **109**, 053309 (2024).
- [34] M. Tylutki, G. E. Astrakharchik, B. A. Malomed, and D. S. Petrov, *Phys. Rev. A* **101**, 051601 (2020).
- [35] G. E. Astrakharchik and B. A. Malomed, *Phys. Rev. A* **98**, 013631 (2018).
- [36] X. Du, Y. Fei, X.-L. Chen, and Y. Zhang, *Phys. Rev. A* **108**, 033312 (2023).
- [37] M. Edmonds, *Phys. Rev. Res.* **5**, 023175 (2023).
- [38] G. C. Katsimiga, S. I. Mistakidis, G. N. Koutsokostas, D. J. Frantzeskakis, R. Carretero-González, and P. G. Kevrekidis, *Phys. Rev. A* **107**, 063308 (2023).
- [39] M. N. Tengstrand and S. M. Reimann, *Phys. Rev. A* **105**, 033319 (2022).
- [40] E. G. Charalampidis and S. I. Mistakidis, *Phys. Rev. A* **111**, 013318 (2025).
- [41] T. Ilg, J. Kumlin, L. Santos, D. S. Petrov, and H. P. Büchler, *Phys. Rev. A* **98**, 051604 (2018).
- [42] P. Zin, M. Pylak, T. Wasak, M. Gajda, and Z. Idziaszek, *Phys. Rev. A* **98**, 051603 (2018).
- [43] L. Lavoine and T. Bourdel, *Phys. Rev. A* **103**, 033312 (2021).
- [44] S. I. Mistakidis, T. Mithun, P. G. Kevrekidis, H. R. Sadeghpour, and P. Schmelcher, *Phys. Rev. Res.* **3**, 043128 (2021).
- [45] I. A. Englezos, S. I. Mistakidis, and P. Schmelcher, *Phys. Rev. A* **107**, 023320 (2023).
- [46] I. A. Englezos, P. Schmelcher, and S. I. Mistakidis, *Phys. Rev. A* **110**, 023324 (2024).
- [47] L. Parisi, G. E. Astrakharchik, and S. Giorgini, *Phys. Rev. Lett.* **122**, 105302 (2019).
- [48] L. Parisi and S. Giorgini, *Phys. Rev. A* **102**, 023318 (2020).
- [49] I. A. Englezos, P. Schmelcher, and S. I. Mistakidis, *SciPost Phys.* **19**, 133 (2025).
- [50] P. Kaur, A. Roy, and S. Gautam, *Comput. Phys. Commun.* **259**, 107671 (2021); P. Banger, P. Kaur, A. Roy, and S. Gautam, *Comput. Phys. Commun.* **279**, 108442 (2022); P. Banger, P. Kaur, and S. Gautam, *Int. J. Mod. Phys. C* **33**, 2250046 (2021).
- [51] A. Roy, S. Pal, S. Gautam, D. Angom, and P. Muruganandam, *Comput. Phys. Commun.* **256**, 107288 (2020); P. Banger, Rajat, and S. Gautam, *Phys. Rev. A* **111**, 023311 (2025).
- [52] P. Zin, M. Pylak, and M. Gajda, *New Journal of Physics* **23**, 033022 (2021).
- [53] S. V. Rajat, S. Gautam, and A. Roy, arXiv:2510.11671 (2025).
- [54] P. Banger, Rajat, A. Roy, and S. Gautam, *Phys. Rev. A* **108**, 043310 (2023).
- [55] H. Xiao, X. Zhang, J. Liu, X. Du, X.-L. Chen, and Y. Zhang, arXiv:2601.16808 (2026).